

Investigating a new neutral heavy gauge boson within the mono-Z' model via simulated pp collisions at $\sqrt{s} = 14$ TeV at the HL-LHC.

Ali Muhammad H. H.*

*Physics Department, Faculty of Science, Ain Shams University, Cairo,
Basic Science Department, Faculty of Engineering, The British University in Egypt, Cairo*

El-sayed A. El-dahshan

Physics Department, Faculty of Science, Ain Shams University, Cairo

S. Elgammal

Centre for Theoretical Physics, The British University in Egypt, Cairo

In this study, we aim to explore the potential for generating events related to dark matter (DM) in conjunction with a neutral heavy gauge boson (Z') decaying leptonically during proton-proton collisions at the Large Hadron Collider (LHC). These collisions occur at a center-of-mass energy of $\sqrt{s} = 14$ TeV, with a high integrated luminosity equivalent to 1000 fb^{-1} . Our analysis involves interpreting the outcomes through Monte Carlo simulation of the effective field theory (EFT) framework. If no new physics is detected, we establish constraints on various parameters within the EFT context, such as the scenario cutoff scale (Λ) and the Z' mass.

Keywords: The High-Luminosity Large Hadron Collider HL-LHC, Large Hadron Collider LHC, New neutral heavy gauge boson, The Compact Muon Solenoid CMS, Dark matter

I. INTRODUCTION

There is a strong belief in scientific circles, based on astronomical observations, that the known baryonic matter is not the whole story and only forms about 27% of the universe's mass [1–9]. The rest is attributed to dark energy and dark matter. This mystery of dark matter has been an ongoing research point for astronomers and particle physicists on equal feet for decades. That is why CERN dedicated two of its Large Hadron Collider (LHC) experiments (i.e. CMS, and ATLAS) to solving this mystery.

The most prosperous theory in particle physics is the standard model of particle physics (SM), in which two of the four fundamental forces, electromagnetism, and the weak nuclear force, are unified in one entity called the electroweak force [10]. Although this theory has accomplished great success, the last of them was the discovery of the Higgs boson at the LHC in 2012 by ATLAS and CMS collaborations [11], it fails to answer a wide range of questions of interest, including what particles form dark matter [10, 12].

Many theorists have proposed various theories beyond the standard model (BSM) hoping to extend the success of the SM to more than discovering the Higgs particle and being obsessed with finding the dark matter particles [12]. The promising BSM models, referred to as "mono-X" models, make predictions about possible occurrences involving the production of dark matter in association with a visible particle. Which acts as a candle, single photon, quark, or gauge boson (i.e. Z , W or

Higgs) [13–20]. These occurrences are identified by visible state particles and a substantial amount of missing transverse energy (E_T^{miss}) signifying the presence of dark matter [21]. In alternative models, X might be an unseen particle, such as the heavy neutral gauge boson Z' . One example is the mono- Z' model [22], in which dark matter particles can be generated alongside Z' through three potential scenarios: the light vector (LV), dark Higgs (DH), and effective field theory (EFT). The ATLAS collaboration has investigated the leptonic decay of Z' [23] and its hadronic decay [24]. They thoroughly examined the LV and DH scenarios. Neither the CMS nor ATLAS collaboration has explored the EFT interpretation of the mono- Z' model. In reference [23], they used the full run-2 data taken by the LHC at 13 TeV center-of-mass energy (\sqrt{s}) of proton-proton collisions with an integrated luminosity of 140 fb^{-1} . This search has ruled out Z' masses ranging from 200 to 450 GeV for the heavy dark sector of the LV scenario, taking $g_q = g_l = 0.1$ and $g_D = 1.0$, where g_q , g_l , and g_D are the couplings of the Z' to the SM quarks, leptons, and dark matters, respectively.

This investigation examines the mono- Z' model in the muonic decay channel of the neutral heavy gauge boson Z' . Monte Carlo simulation is utilized to replicate proton-proton collisions at $\sqrt{s} = 14$ TeV with a substantial integrated luminosity of 1000 fb^{-1} at the LHC. This particular range of integrated luminosity at the LHC is referred to as the High-Luminosity Large Hadron Collider (HL-LHC), the upcoming upgrade of the LHC, expected to commence in 2028 [25]. The EFT scenario is the focal point of this study.

The paper is structured as follows: Section II provides a brief explanation of the mono- Z' model and its EFT scenario. Section III briefly introduces the upcoming upgrade of the LHC, known as the HL-LHC project, and the

* Ali.Hamed@bue.edu.eg

Compact Muon Solenoid (CMS) detector. Moving on to the methodology discussion, the simulated signal samples and their SM background sources are discussed in section IV. Following that, in section V, the event selection and the analysis approach are covered. The yielded results and conclusion of the study are presented in section VI and section VII, respectively.

II. THE EFT SCENARIO IN THE CONTEXT OF THE MONO-Z' MODEL

The mono-Z' model, a new model proposed in [22], proposes that dark matter production accompanied by a resonance yielded from a new neutral heavy gauge boson called the Z' is possible. This model comes in three different scenarios: the light vector (LV) scenario, referred to as the dark fermion scenario, the dark Higgs (DH) scenario, and the light vector accompanied by the coupling of inelastic effective field theory (EFT) scenario.

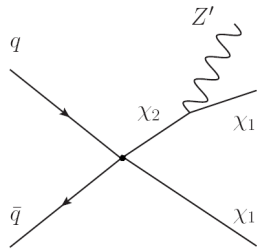


Figure 1 The Feynman diagram for the Effective field theory scenario (EFT) [22].

Scenario	Masses assumptions
Heavy dark sector	$M_{\chi_1} = M_{Z'}/2$ $M_{\chi_2} = 2M_{Z'}$

Table I The heavy dark sector mass assumptions for EFT scenario [22].

The EFT scenario differs from the LV scenario in that the DM and SM particle interactions are reduced to a contact interaction expressed in the Lagrangian interaction term shown in equation (1).

$$\frac{1}{2\Lambda^2} \bar{q} \gamma^\mu q (\bar{\chi}_2 \gamma^\mu \gamma^5 \chi_1 + \bar{\chi}_1 \gamma^\mu \gamma^5 \chi_2). \quad (1)$$

Figure 1 displays the Feynman diagram illustrating the process, and table I points to the dark sector mass assumption used for the process. Throughout this paper, the SM leptons coupling with Z' is denoted as g_l , and the DM particles coupling with the Z' is denoted as g_D . The main free parameters of the EFT scenario in the mono-Z' model are the model cut-off scale (Λ) and the Z' mass

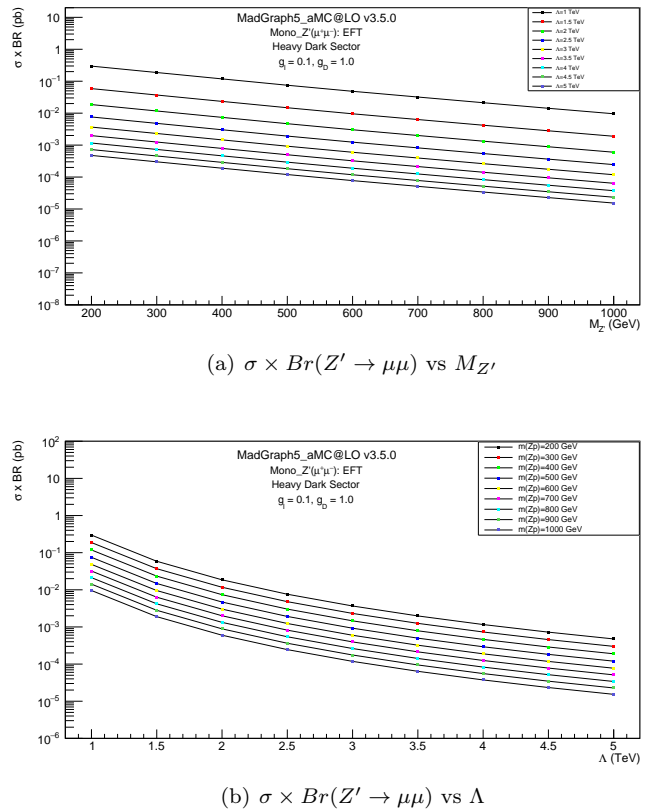


Figure 2 The plots of $\sigma \times Br(Z' \rightarrow \mu\mu)$ for the EFT signal versus $M_{Z'}$ 2(a), and Λ 2(b) regarding the scenario of EFT at $\sqrt{s} = 14$ TeV evaluated using MadGraph5.

($M_{Z'}$). Despite finding that changing g_l changes the corresponding cross-section values, g_l is chosen to be 0.1 to be consistent with the results of the ATLAS collaboration presented in [23].

The study scope is on the Z' decay to dimuon $Z' \rightarrow \mu\bar{\mu}$ by simulating the behavior of the CMS detector. This choice was motivated by the CMS detector's optimization for detecting the muonic decay channel of $Z' \rightarrow \mu\bar{\mu}$. Additionally, we examined the range of masses in the heavy dark sector, as detailed in table I.

The EFT signal events of the model were generated using the general-purpose matrix element event generator known as MadGraph5_aMC@NLO v3.5.0 [26], at $\sqrt{s} = 14$ TeV. Table II lists the measurements of the cross-sections and the branching ratio product for various values of Λ and $M_{Z'}$. These generated data are used to set limits to the free parameters, Λ and $M_{Z'}$, as explained later in the results section.

Figure 2 presents the production of the EFT signal cross-section versus $M_{Z'}$ 2(a) and Λ 2(b) at $\sqrt{s} = 14$ TeV. The cross-section times the branching ratio ($\sigma \times Br(Z' \rightarrow \mu\mu)$) is expected to decrease with the Λ and the mass of the Z'.

Λ (TeV)	200	300	400	500	600	700	800	900	1000	1500	2000
$M_{Z'}$ (GeV)	1	1.87 $\times 10^{-01}$	1.18 $\times 10^{-01}$	7.49 $\times 10^{-02}$	4.84 $\times 10^{-02}$	3.2 $\times 10^{-02}$	2.13 $\times 10^{-02}$	1.42 $\times 10^{-02}$	9.58 $\times 10^{-03}$	1.311 $\times 10^{-03}$	1.692 $\times 10^{-04}$
1.5	5.87 $\times 10^{-02}$	3.7 $\times 10^{-02}$	2.34 $\times 10^{-02}$	1.48 $\times 10^{-02}$	9.56 $\times 10^{-03}$	6.33 $\times 10^{-03}$	4.2 $\times 10^{-03}$	2.81 $\times 10^{-03}$	1.89 $\times 10^{-03}$	2.59 $\times 10^{-04}$	3.342 $\times 10^{-05}$
2	1.86 $\times 10^{-02}$	1.17 $\times 10^{-02}$	7.39 $\times 10^{-03}$	4.68 $\times 10^{-03}$	3.02 $\times 10^{-03}$	2 $\times 10^{-03}$	1.33 $\times 10^{-03}$	8.88 $\times 10^{-04}$	5.99 $\times 10^{-04}$	8.173 $\times 10^{-05}$	1.061 $\times 10^{-05}$
2.5	7.61 $\times 10^{-03}$	4.8 $\times 10^{-03}$	3.03 $\times 10^{-03}$	1.92 $\times 10^{-03}$	1.24 $\times 10^{-03}$	8.2 $\times 10^{-04}$	5.44 $\times 10^{-04}$	6.64 $\times 10^{-04}$	2.45 $\times 10^{-04}$	3.352 $\times 10^{-05}$	4.344 $\times 10^{-06}$
3	3.67 $\times 10^{-03}$	2.31 $\times 10^{-03}$	1.46 $\times 10^{-03}$	9.25 $\times 10^{-04}$	5.97 $\times 10^{-04}$	3.95 $\times 10^{-04}$	2.62 $\times 10^{-04}$	1.76 $\times 10^{-04}$	1.18 $\times 10^{-04}$	1.617 $\times 10^{-05}$	2.095 $\times 10^{-06}$
3.5	1.98 $\times 10^{-03}$	1.25 $\times 10^{-03}$	7.88 $\times 10^{-04}$	4.99 $\times 10^{-04}$	3.23 $\times 10^{-04}$	2.13 $\times 10^{-04}$	1.42 $\times 10^{-04}$	9.47 $\times 10^{-05}$	6.39 $\times 10^{-05}$	8.724 $\times 10^{-06}$	1.131 $\times 10^{-06}$
4	1.16 $\times 10^{-03}$	7.32 $\times 10^{-04}$	4.62 $\times 10^{-04}$	2.93 $\times 10^{-04}$	1.89 $\times 10^{-04}$	1.25 $\times 10^{-04}$	8.3 $\times 10^{-05}$	5.55 $\times 10^{-05}$	3.74 $\times 10^{-05}$	5.128 $\times 10^{-06}$	6.638 $\times 10^{-07}$
4.5	7.25 $\times 10^{-04}$	4.57 $\times 10^{-04}$	2.88 $\times 10^{-04}$	1.83 $\times 10^{-04}$	1.18 $\times 10^{-04}$	7.81 $\times 10^{-05}$	5.18 $\times 10^{-05}$	3.47 $\times 10^{-05}$	2.34 $\times 10^{-05}$	3.206 $\times 10^{-06}$	4.149 $\times 10^{-07}$
5	4.75 $\times 10^{-04}$	3 $\times 10^{-04}$	1.89 $\times 10^{-04}$	1.2 $\times 10^{-04}$	7.74 $\times 10^{-05}$	5.12 $\times 10^{-05}$	3.4 $\times 10^{-05}$	2.27 $\times 10^{-05}$	1.53 $\times 10^{-05}$	2.091 $\times 10^{-06}$	2.716 $\times 10^{-07}$
10	2.971 $\times 10^{-05}$	1.874 $\times 10^{-05}$	1.183 $\times 10^{-05}$	7.493 $\times 10^{-06}$	4.838 $\times 10^{-06}$	3.202 $\times 10^{-06}$	2.126 $\times 10^{-06}$	1.421 $\times 10^{-06}$	9.583 $\times 10^{-07}$	1.307 $\times 10^{-07}$	1.702 $\times 10^{-08}$
13	1.04 $\times 10^{-05}$	6.561 $\times 10^{-06}$	4.139 $\times 10^{-06}$	2.624 $\times 10^{-06}$	1.694 $\times 10^{-06}$	1.121 $\times 10^{-06}$	7.443 $\times 10^{-07}$	4.997 $\times 10^{-07}$	3.355 $\times 10^{-07}$	4.576 $\times 10^{-08}$	5.958 $\times 10^{-09}$

Table II The readings of product of the EFT cross-section and branching ratio measured in (pb) regarding various values of $M_{Z'}$ and Λ in GeV and TeV, respectively, in the heavy dark sector, using the coupling constants values $g_D = 1.0$, $g_l = 0.1$, at $\sqrt{s} = 14 \text{ TeV}$.

III. THE HL-LHC PROJECT

Several upgrades have been conducted to the LHC, including Run I, Run II, and Run III, making it a worthy investment. The next upgrade, the HL-LHC, will increase the energy and the number of collisions, producing more data for statistical studies and accuracy. This upgrade requires new equipment to be installed over 1.2 km of the 27 km long LHC [25].

The CMS detector, a primary detector at CERN's LHC, aims to search for new physics using its complex structure. It employs different-angle concepts in its measurements, including the polar angle (θ), the azimuthal angle (ϕ), and the pseudo-rapidity (η).

The CMS detector coordinate system is as follows: the z-axis runs along the beam axis of the colliding particles, the x-axis is directed toward the LHC center, and the y-axis is directed upwards. The measurement of ϕ is in the x-y transverse plane, while the measurement of θ is along the x-axis. Nevertheless, the direction of the colliding particles' products regarding the collision spot is described using η , defined as $\eta = -\ln[\tan(\theta/2)]$ [27–29].

IV. MONTE CARLO SAMPLES SIMULATION

A. The Signal Samples Simulations

The signal events of the model were generated using MadGraph5_aMC@NLO v3.5.0 [26]. The next-to-leading-order (NLO) is used in cross-section calculations at $\sqrt{s} = 14 \text{ TeV}$, and Pythia8 [30] is used for hadronization and parton showering processes. For fast detector simulation for CMS experiment, DELPHES [31] has been used. The EFT production cross-section calculations have been scanned for an extensive variety of the $M_{Z'}$ ranging from 200 GeV to 2000 GeV, and for Λ from 1 TeV to 5 TeV assuming the coupling constants values are $g_l = 0.1$, and $g_D = 1.0$ as those used in [23, 24].

B. The Simulation of SM Backgrounds

In this analysis, the studied EFT signal topology is dimuon plus missing transverse energy ($\mu^+ \mu^- + E_T^{miss}$). Therefore, several SM processes could mimic this topology via having muons and/or E_T^{miss} , arising from undetected neutrinos, in their final states. Such interactions are considered SM backgrounds for the signal. Those SM backgrounds are The Drell-Yan (DY) process ($DY \rightarrow \mu^+ \mu^-$), the fully leptonic decay of top-quark pairs ($t\bar{t} \rightarrow \mu^+ \mu^- + 2b + 2\nu$), the single top process ($\bar{t}W^+ \rightarrow \mu^+ \mu^- + 2b + 2\nu$, $tW^- \rightarrow \mu^+ \mu^- + 2b + 2\nu$), and the electroweak diboson channels production ($W^+W^- \rightarrow \mu^+ \mu^- + 2\nu$, $W^\pm Z \rightarrow \mu^\pm \mu^\pm \mu^- + \nu$, $ZZ \rightarrow \mu^+ \mu^- + 2\nu$, and $ZZ \rightarrow \mu^+ \mu^- \mu^+ \mu^-$). All these Monte Carlo Samples have a cross-section calculated at NLO using MadGraph5_aMC@NLO v3.5.0 [26] interfaced with

Pythia8 [30] for hadronization and modeling. All contributions of SM background processes and signal samples are estimated using Monte Carlo Simulation and normalized to their corresponding cross-section and 1000 fb^{-1} integrated luminosity.

V. SELECTION OF EVENTS

In this analysis, the event selection is designed to reconstruct two-high- p_T muons of opposite charges associated with E_T^{miss} , referring to DM candidates, in the final state. This selection is presented as applied cuts to different kinematics requiring muons to pass the preliminary selection shown in table III. Thus, each muon should be with $p_T^\mu > 30 \text{ GeV}$ and $|\eta^\mu| < 2.4$, in addition, this muon must be isolated and pass the following criteria "IsolationVarRhoCorr" referring to the isolation cut in DELPHES to eliminate muons produced inside jets. For this cut, corrected for the pileup effect, the scalar summation of the p_T of all the tracks of muons should not go beyond 10% of the muon p_T^μ . This must be in the limits of a $\Delta R = 0.5$ cone surrounding the muon candidate, except the candidate itself. The dimuon invariant mass is greater than 60 GeV as we search for a high mass regime resonance.

Figure 3(a) displays the histograms of the dimuon invariant mass distribution for the signal and the stacked background histograms. The blue histogram, the dominant background, refers to the DY background, while the yellow one is for the electroweak background of vector boson pairs (ZZ, WW, and WZ). The backgrounds of the top-quark pair ($t\bar{t}$), and the single top (tW) are denoted by the red histogram. The different colored lines overlaid on the stacked histograms of the background represent the EFT signal, generated for different values of the $M_{Z'}$, in the heavy-dark sector masses assumptions and a fixed value of $\Lambda = 1 \text{ TeV}$. The corresponding E_T^{miss} distribution is illustrated in figure 3(b).

In figures 3(a) and 3(b), as the background overwhelms the signal, we need a tighter set of discrimination cuts to distinguish between the signals and the SM backgrounds. We have four-cut parameters: the first one is the requirement of the dimuon invariant mass to be restricted to a small range of the $M_{Z'}$, where $0.9 \times M_{Z'} < M_{\mu^+\mu^-} < M_{Z'} + 25$ as recommended by [22]. Secondly is the selection of the relative difference of the dimuon transverse energy ($E_T^{\mu^+\mu^-}$) and the E_T^{miss} to be less than 0.4 (i.e. $|E_T^{\mu^+\mu^-} - E_T^{\text{miss}}| / E_T^{\mu^+\mu^-} < 0.4$). The third parameter is the cone radius $\Delta R(\mu^+\mu^-)$ to be less than 3.2 (i.e. $\Delta R(\mu^+\mu^-) < 3.2$). The fourth and last parameter is the azimuthal angle between the dimuon and the E_T^{miss} directions, defined as $\Delta\Phi_{\mu^+\mu^-, E_T^{\text{miss}}} = |\Phi^{\mu^+\mu^-} - \Phi^{\text{miss}}|$, to be selected as $\Delta\Phi_{\mu^+\mu^-, E_T^{\text{miss}}} > 2.6$. Table III summarizes these selection criteria.

Figure 4 shows the distributions, scaled to one, of $|E_T^{\mu^+\mu^-} - E_T^{\text{miss}}| / E_T^{\mu^+\mu^-}$ 4(a), $\Delta\Phi_{\mu^+\mu^-, E_T^{\text{miss}}}$ 4(b), and

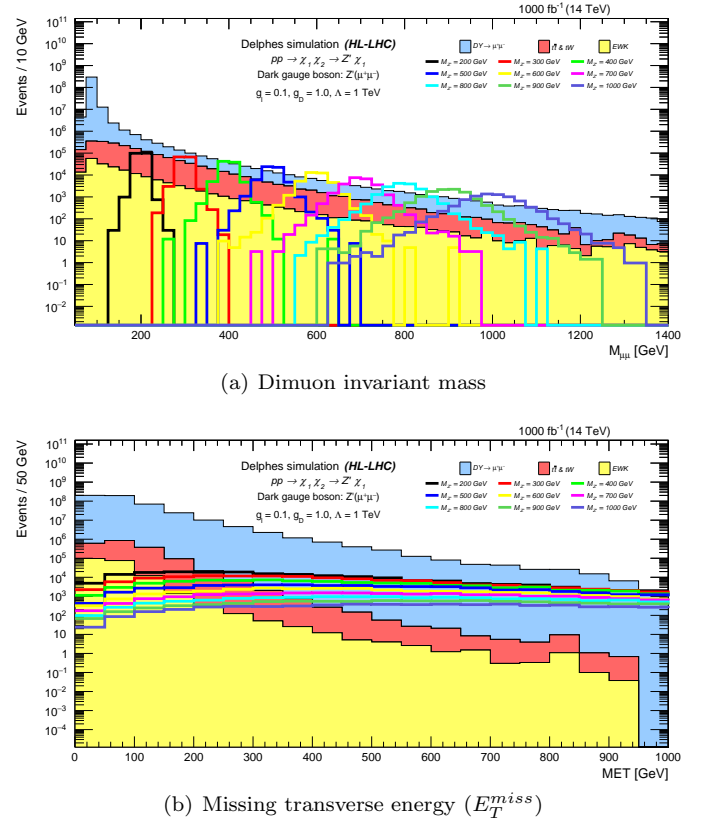


Figure 3 The histograms of the dimuon invariant mass 3(a), and the missing transverse energy 3(b) distributions regarding the expected SM background and the EFT scenario signal of different $M_{Z'}$ values in the heavy-dark sector at $\Lambda = 1 \text{ TeV}$ after applying the preliminary selection, listed in table III.

$\Delta R(\mu^+\mu^-)$ 4(c) with their corresponding cutting values for dimuons events applied to the SM background and the generated signal of the EFT scenario in the heavy dark sector for $M_{Z'} = 200 \text{ GeV}$ and $\Lambda = 1 \text{ TeV}$. The application of the mass window cut ($0.9 \times M_{Z'} < M_{\mu^+\mu^-} < M_{Z'} + 25$) fully suppresses the $ZZ \rightarrow \mu^+\mu^- + 2\nu$ background. The next section presents the results of applying these cuts to the E_T^{miss} showing how strongly these cuts reduced the SM background for the sake of discrimination between the signal and the SM background.

VI. RESULTS

The shape-based analysis is chosen to be based on the E_T^{miss} distribution because of the good discrimination it gives between the signal of the model and the SM background combination. Figure 5 displays the invariant mass distribution of the dimuon pairs, related to the production of Z' , after applying the preliminary and tight cuts, listed in table III, except the mass window cut. As noticed, there is a significant decrease in the SM back-

Step	Criteria	Requirements
Preliminary selection	p_T^μ (GeV)	> 30
	$ \eta^\mu $ (rad)	< 2.4
	IsolationVarRhoCorr	< 0.1
	$M_{\mu^+\mu^-}$ (GeV)	> 60
Tight selection	$\Delta R(\mu^+\mu^-)$	< 3.2
	$\Delta\phi_{\mu^+\mu^-, \vec{E}_T^{\text{miss}}}$	> 2.6
	$ E_T^{\mu^+\mu^-} - E_T^{\text{miss}} /E_T^{\mu^+\mu^-}$	< 0.4
	Mass window (GeV)	$0.9 \times M_{Z'} < M_{\mu^+\mu^-} < M_{Z'} + 25$

Table III Summary of the preliminary and tight cuts of the final event selection used in this cut-based analysis.

grounds while preserving the signal strength, as demonstrated by the comparison of figures 3(a) and 5 for the EFT scenario.

Figure 6 illustrates the E_T^{miss} distribution after applying the all cuts presented in table III.

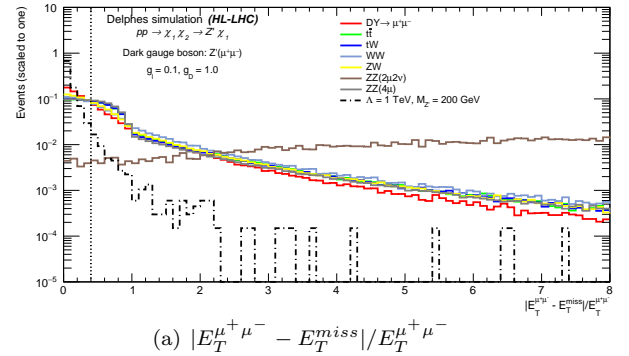
This analysis also introduces a calculation of the signal statistical significance (S) over the SM backgrounds using the Asimov formula, equation (2), described in [32].

$$S = \sqrt{2 \times ((N_s + N_b) \log(1 + \frac{N_s}{N_b}) - N_s)}, \quad (2)$$

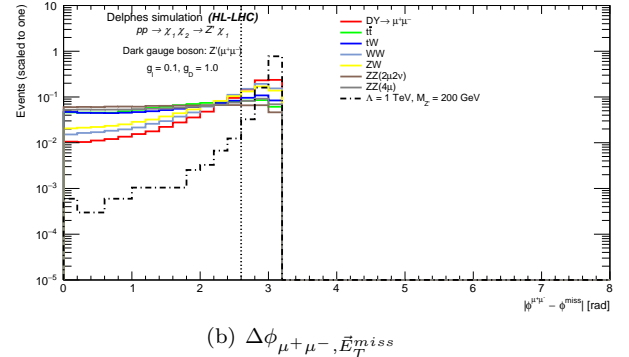
where N_s and N_b are the number of events of the signal and the total SM backgrounds, respectively, passing the final selections shown in table III.

This investigation assessed the significance at the five sigma level (5σ) with high integrated luminosity values for the EFT scenario at $\sqrt{s} = 14$ TeV. We explored different values of Λ while keeping the Z' mass fixed at $M_{Z'} = 600$ GeV in 7(a), and we also examined various values of $M_{Z'}$ with Λ fixed at $\Lambda = 4$ TeV in 7(b). Our findings revealed that a 5σ significance can be achieved at an integrated luminosity of about 1900 fb^{-1} for $M_{Z'} = 600$ GeV and $\Lambda = 4$ TeV, as illustrated in figure 7.

The statistical results for these outcomes were derived by conducting a statistical analysis using the profile likelihood method. Additionally, The modified frequentist construction confidence levels (CLs) are used, as outlined in references [33–35]. These methods were employed to establish the limits excluded for the $\sigma \times Br(Z' \rightarrow \mu\mu)$ of the generated EFT signals with a 95% CL.



(a) $|E_T^{\mu^+\mu^-} - E_T^{\text{miss}}|/E_T^{\mu^+\mu^-}$



(b) $|\phi^{\mu^+} - \phi^{\mu^-}|$

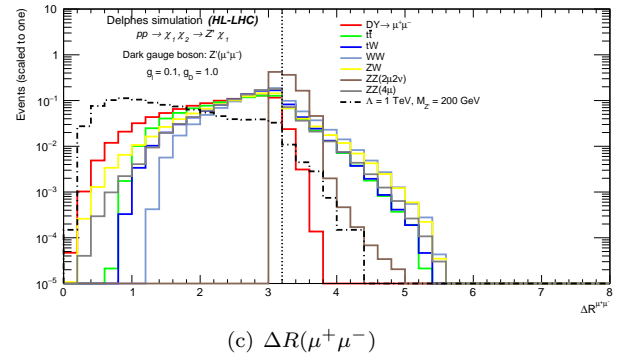


Figure 4 The histograms correspond to the EFT scenario signal ($\Lambda = 1$ TeV, and $M_{Z'} = 200$ GeV), and SM backgrounds. The histograms are normalized to unity to highlight qualitative features, and the vertical dashed lines correspond to the chosen cut value per each variable.

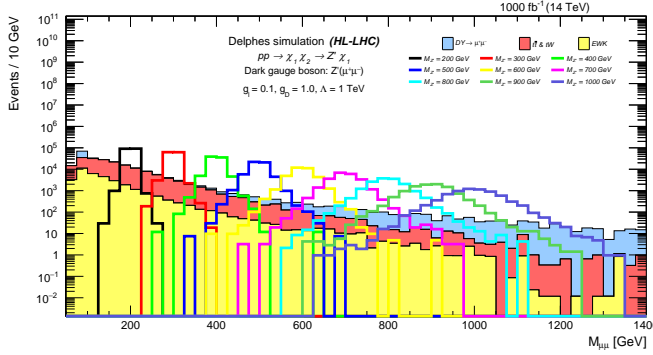


Figure 5 The histograms of dimuon invariant mass for the anticipated SM backgrounds and the generated signal of the EFT scenario for $M_{Z'} = 200$ GeV in the heavy-dark sector at $\Lambda = 1$ TeV after applying all cuts, listed in table III, except the mass window cut

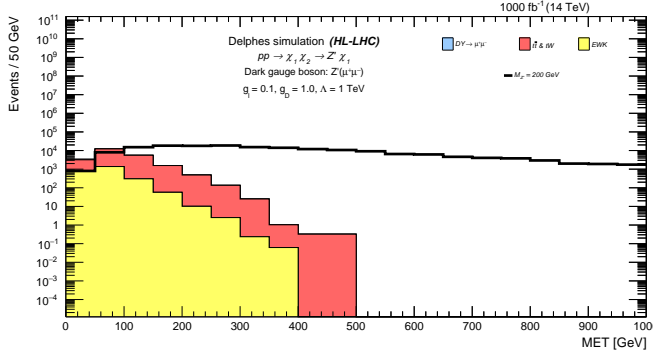
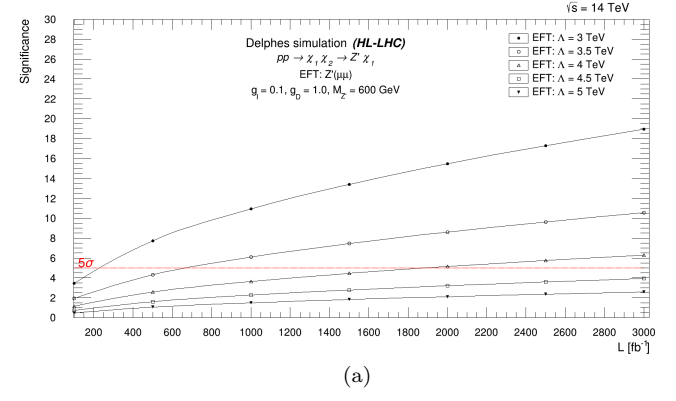


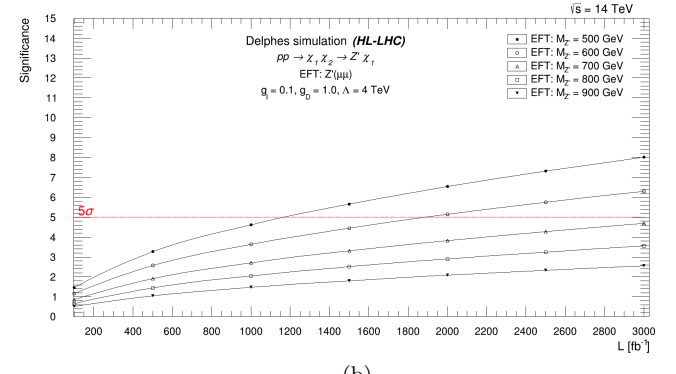
Figure 6 The histograms of the missing transverse energy regarding the anticipated SM background and the generated signal of the EFT scenario for $M_{Z'} = 200$ GeV in the heavy-dark sector at $\Lambda = 1$ TeV after applying all cuts, listed in table III.

In Figure 8 illustrates the 95% upper limit on $\sigma \times Br(Z' \rightarrow \mu\mu)$ plotted against $M_{Z'}$ for the EFT scenario based on the mono-Z' model. This specifically pertains to the muonic decay of Z' and the values of the coupling constants ($g_D = 1.0$, $g_l = 0.1$) in the heavy dark sector, as detailed in table I, for various Λ values. The solid black curve in these five plots represents the theoretical $\sigma \times Br(Z' \rightarrow \mu\mu)$ of the EFT scenario for a specific value of Λ . Based on the plots in figure 8, the production of the Z' is ruled out in the mass range of 200 to 2000 GeV for $\Lambda = 1$ TeV 8(a) and 1.5 TeV 8(b), from 200 to 1929 GeV for $\Lambda = 2$ TeV 8(c), and from 200 to 1305 GeV for $\Lambda = 4$ TeV 8(d) as indicated from the expected median.

Figure 9 presents the anticipated exclusion limits at a 95% CL resulting from the EFT scenario search with 1000 fb^{-1} of 14 TeV proton-proton collision simulated data. These limits are presented as a function of $M_{Z'}$ and Λ . The colored region represents the upper limit, while a dashed black line denotes the median of the expected limits.



(a)



(b)

Figure 7 The five sigma significance of the EFT scenario versus the HL-LHC integrated luminosity plotted for different values of Λ at $M_{Z'} = 600$ GeV in 7(a), and for several values of $M_{Z'}$ at $\Lambda = 4$ TeV in 7(b).

VII. SUMMARY

This study proposed a search for a Z' boson decaying into dimuon in association with neutral particles (dark matter particles χ_1 and χ_2) in the framework of the EFT scenario.

Monte Carlo simulations of proton-proton collisions at $\sqrt{s} = 14$ TeV for 1000 fb^{-1} integrated luminosity, corresponding to the HL-LHC project were used. The analysis presented results of the muonic decay of Z' for the heavy dark sector ($M_{\chi_1} = M_{Z'}/2$, and $M_{\chi_2} = 2M_{Z'}$), given that the coupling constants are fixed and chosen to be $g_l = 0.1$ and $g_D = 1.0$. 95% CL limit on the model's free parameters are shown for Λ and $M_{Z'}$.

A previous study by the ATLAS collaboration [23], has used the full run-2 data taken by the LHC at $\sqrt{s} = 13$ TeV of proton-proton collisions with an integrated luminosity of 140 fb^{-1} . Which has excluded Z' masses ranging from 200 to 450 GeV within the heavy dark sector of the LV scenario for $g_q = g_l = 0.1$ and $g_D = 1.0$. While, this study has shown that a wider range of Z' mass spectrum, 200 GeV to 2000 GeV, can be excluded for $\Lambda = 1$ and 1.5 TeV with the increase of the LHC center of mass en-

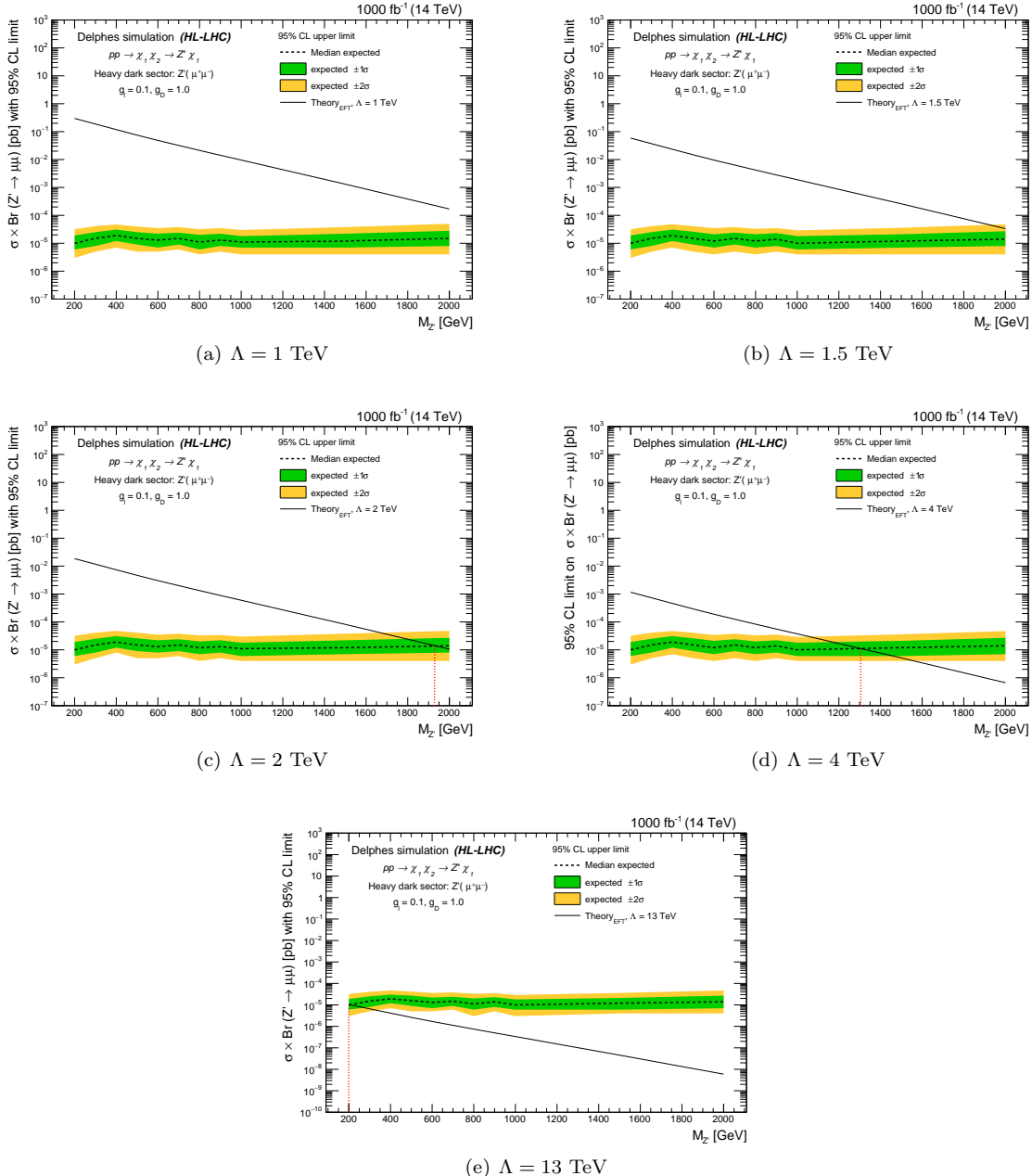


Figure 8 The 95% CL expected limit on $\sigma \times Br(Z' \rightarrow \mu\mu)$, versus $M_{Z'}$ for the muonic decay of the Z' in the EFT scenario which is referred to by a solid black line with $\Lambda = 1$ TeV 8(a), 1.5 TeV 8(b), 2 TeV 8(c), 4 TeV 8(d), and 13 TeV 8(e). The vertical dotted red line refers to the upper limit value.

ergy from 13 to 14 TeV. For very high values of the EFT cutoff scale (i.e. $\Lambda > 13$ TeV), the HL-LHC will not be sensitive to the EFT scenario.

The two-dimensional exclusion as a function of $M_{Z'}$ and Λ has shown that $M_{Z'}$ up to 2 TeV and Λ up to 13 TeV will be probed.

VIII. ACKNOWLEDGMENTS

The author of this paper appreciates the help Tongyan Lin, an author in [22], for sending us the Universal Feyn-Rules Output (UFO) file for the model used in the generation of the events. We also want to thank Mahmoud Hashim for his help with the IT issues faced throughout this work.

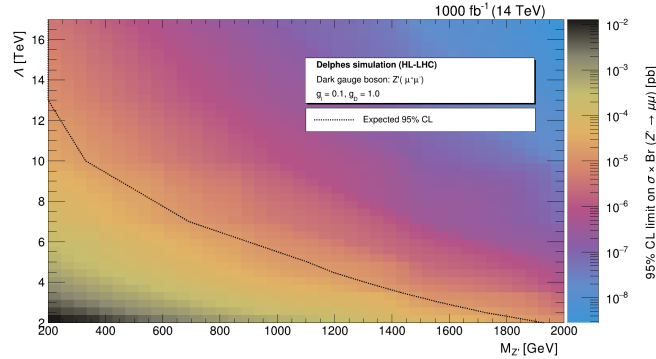


Figure 9 The upper limits at a 95% CL on $\sigma \times Br(Z' \rightarrow \mu\mu)$ are determined from the inclusive search, considering different pairs of EFT scenario parameters (Λ and $M_{Z'}$). The colored region represents the upper limit, while the dashed black line shows the expected exclusions for the nominal Z' cross-section.

[1] F. Zwicky, *Helv. Phys. Acta* 6, 110 (1933).

[2] R. J. Scherrer and M. S. Turner, *Phys. Rev. D* 33, 1585 (1986).

[3] P. A. R. Ade et al., *Astron. Astrophys.* 594, A13 (2016).

[4] Y. Sofue and V. Rubin, *Annu. Rev. Astron. Astrophys.* 39, 137 (2001).

[5] V. Trimble, *Annu. Rev. Astron. Astrophys.* 25, 425 (1987).

[6] G. Bertone, D. Hooper, and J. Silk, *Phys. Rep.* 405, 279 (2005).

[7] L. Bergström, *Rep. Prog. Phys.* 63, 793 (2000).

[8] K. Abazajian, G. M. Fuller, and M. Patel, *Phys. Rev. D* 64, 023501 (2001).

[9] C. Lage and G. R. Farrar, *J. Cosmol. Astropart. Phys.* 2015, 038 (2015).

[10] G. Ross, *Nature* 311, 5986 (1984).

[11] S. Chatrchyan et al., *Phys. Lett. B* 716, 30 (2012).

[12] P. Langacker, *The Standard Model and Beyond* (Taylor & Francis, 2017).

[13] CMS Collaboration, [arXiv:1810.00196](#) [hep-ex] (2018).

[14] CMS Collaboration, [arXiv:1901.01553](#) [hep-ex] (2019).

[15] A. Tumasyan et al., *J. High Energy Phys.* 2021, 11 (2021) 1-72.

[16] CMS Collaboration, *Eur. Phys. J. C* 81, 13 (2021).

[17] CMS Collaboration, [arXiv:2201.11585](#) [hep-ex] (2022).

[18] A. Hayrapetyan et al., *J. High Energy Phys.* 2024, 3 (2024) 1-45.

[19] S. Belforte et al., *Phys. Rev. Lett.* 132, 041801 (2024).

[20] CMS Collaboration, *Eur. Phys. J. C* 79, 280 (2019).

[21] CMS Collaboration, [arXiv:1605.09305](#) [hep-ex] (2016).

[22] M. Autran et al., *Phys. Rev. D* 92, 035007 (2015).

[23] ATLAS Collaboration, [arXiv:2303.XXXX](#) [hep-ex] (2023).

[24] M. Aaboud et al., *J. High Energy Phys.* 2018, 10 (2018) 1-58.

[25] O. Brüning and L. Rossi, in *The High Luminosity Large Hadron Collider: New Machine for Illuminating the Mysteries of the Universe*, edited by T. Dumont and L. Rossi (2024), pp. 1-53.

[26] J. Alwall et al., *J. High Energy Phys.* 2014, 07 (2014) 1-157.

[27] G. Grégoire et al., *J. Instrum.* 3, S08004 (2008).

[28] CMS Collaboration, *J. Instrum.* 3, S08004 (2008).

[29] G. L. Bayatian, *J. Phys. G* 34, CERN-LHCC-2006-021; CMS-TDR-008-2; FERMILAB-CONF-07-831-CMS (2007).

[30] T. Sjöstrand, S. Mrenna, and P. Skands, *J. High Energy Phys.* 2006, 05 (2006) 026.

[31] J. de Favereau et al., *J. High Energy Phys.* 2014, 02 (2014) 1-26.

[32] G. Cowan and E. Gross, *ATLAS Statistics Forum*, Vol. 8, 2008.

[33] A. L. Read, *J. Phys. G* 28, 2693 (2002).

[34] T. Junk, *Nucl. Instrum. Methods Phys. Res. A* 434, 435 (1999).

[35] G. Cowan et al., *Eur. Phys. J. C* 71, 1554 (2011).